1-1-2013

Effects of tungsten addition on the microstructure and mechanical properties of microalloyed forging steels

Jingwei Zhao
University of Wollongong, jzhao@uow.edu.au

Taekyung Lee
Pohang University of Science and Technology

Jeong Hun Lee
Pohang University of Science and Technology

Zhengyi Jiang
University of Wollongong, jiang@uow.edu.au

Chong Soo Lee
Pohang University of Science and Technology, cslee@postech.ac.kr

Effects of tungsten addition on the microstructure and mechanical properties of microalloyed forging steels

Abstract

In the current study, the effects of tungsten (W) addition on the microstructure, hardness, and room/low [223 K and 173 K (-50 C and -100 C)] temperature tensile properties of microalloyed forging steels were systematically investigated. Four kinds of steel specimens were produced by varying the W additions (0, 0.1, 0.5, and 1 wt pct). The microstructure showed that the addition of W does not have any noticeable effect on the amount of precipitates. The precipitates in W-containing steels were all rich in W, and the W concentration in the precipitates increased with the increasing W content. The mean sizes of both austenite grains and precipitates decreased with the increasing W content. When the W content was equal to or less than 0.5 pct, the addition of W favored the formation of allotriomorphic ferrite, which subsequently promoted the development of acicular ferrite in the microalloyed forging steels. The results of mechanical tests indicated that W plays an important role in increasing the hardness and tensile strength. When the testing temperature was decreased, the tensile strength showed an increasing trend. Both the yield strength and the ultimate tensile strength obeyed an Arrhenius type of relation with respect to temperature. When the temperature was decreased from 223 K to 173 K (from -50 C to -100 C), a ductile-to-brittle transition (DBT) of the specimen with 1 pct W occurred. The addition of W favored a higher DBT temperature. From the microstructural and mechanical test results, it is demonstrated that the addition of 0.5 pct W results in the best combination of excellent room/low-temperature tensile strength and ductility. 2013 The Minerals, Metals & Materials Society and ASM International.

Keywords

microalloyed, forging, effects, steels, tungsten, addition, microstructure, mechanical, properties

Disciplines

Engineering | Science and Technology Studies

Publication Details

Zhao, J., Lee, T., Lee, J., Jiang, Z. & Lee, C. Soo. (2013). Effects of tungsten addition on the microstructure and mechanical properties of microalloyed forging steels. Metallurgical and Materials Transactions A: Physical Metallurgy and Materials Science, 44 (8), 3511-3523.

Effects of Tungsten Addition on the Microstructure and Mechanical Properties of Microalloyed Forging Steels

JINGWEI ZHAO, TAEKYUNG LEE, JEONG HUN LEE, ZHENGYI JIANG, and CHONG SOO LEE

In the current study, the effects of tungsten (W) addition on the microstructure, hardness, and room/low [223 K and 173 K (−50 °C and −100 °C)] temperature tensile properties of microalloyed forging steels were systematically investigated. Four kinds of steel specimens were produced by varying the W additions (0, 0.1, 0.5, and 1 wt pct). The microstructure showed that the addition of W does not have any noticeable effect on the amount of precipitates. The precipitates in W-containing steels were all rich in W, and the W concentration in the precipitates increased with the increasing W content. The mean sizes of both austenite grains and precipitates decreased with the increasing W content. When the W content was equal to or less than 0.5 pct, the addition of W favored the formation of allotriomorphic ferrite, which subsequently promoted the development of acicular ferrite in the microalloyed forging steels. The results of mechanical tests indicated that W plays an important role in increasing the hardness and tensile strength. When the testing temperature was decreased, the tensile strength showed an increasing trend. Both the yield strength and the ultimate tensile strength obeyed an Arrhenius type of relation with respect to temperature. When the temperature was decreased from 223 K to 173 K (from −50 °C to −100 °C), a ductile-to-brittle transition (DBT) of the specimen with 1 pct W occurred. The addition of W favored a higher DBT temperature. From the microstructural and mechanical test results, it is demonstrated that the addition of 0.5 pct W results in the best combination of excellent room/low-temperature tensile strength and ductility.

DOI: 10.1007/s11661-013-1695-x

I. INTRODUCTION

FOR saving energy and production costs, the conventional quenched and tempered steels have been successfully replaced by microalloyed forging steels.[1] The strength levels and other properties of microalloyed forging steels achieved after cooling from hot working temperature have been reported to be comparable with those obtained from conventional quenched and tempered steels.[2,3] In microalloyed steels, the addition of a small amount of alloying elements such as titanium (Ti), niobium (Nb), or vanadium (V) offers an important cost-effective approach to obtain a good combination of excellent toughness and strength through grain size control and precipitation hardening.[4–7] A variety of microstructures in microalloyed steels can be obtained depending on the chemical composition and manufacturing procedures. Studies on the microstructure of microalloyed steels with a view to improving their mechanical properties had been conducted by many researchers.[8–10]

Steels used for large-scale structures, such as the tower flanges of wind turbines, are usually produced by hot forging followed by air cooling. For meeting the structural safety requirements, such structural steels require excellent strength to bear static and dynamic heavy loads. For improving load bearing, recent approaches have been focused on developing low-carbon microalloyed steels with good combinations of fracture resistance and strength for the given applications to reduce section size and weight.[11–13] The air-cooled microstructure of microalloyed forging steels is generally composed of ferrite and pearlite. The content, size, and distribution of ferrite and pearlite grains within the microstructure play an important role in the final mechanical properties.[3] Each of the microstructural variables is highly influenced by the chemical composition and forging technology. The chemical composition affects the ferrite volume fraction, the pearlite lath thickness and spacing, the solid solution strengthening effect, and the extent of microalloy precipitation. In the case of the forging technology, these microstructural variables can be accurately correlated to the final microstructure, and consequently to the final mechanical properties, by precisely controlling the chemical compositions of the microalloyed steels. Microalloying modification has become an important issue for improving the mechanical properties of microalloyed forging

JINGWEI ZHAO, Associate Research Fellow, and ZHENGYI JIANG, Professor, are with the School of Mechanical, Materials and Mechatronic Engineering, University of Wollongong, NSW 2522, Australia. TAEKYUNG LEE and JEONG HUN LEE, Ph.D. Candidates, and CHONG SOO LEE, Professor, are with the Department of Materials Science and Engineering and the Graduate Institute of Ferrous Technology, Pohang University of Science and Technology, Pohang 790-784, Republic of Korea. Contact e-mail: cslee@postech.ac.kr

Manuscript submitted June 12, 2012.
Article published online March 20, 2013

steels, and several attempts have been made to achieve this goal.[14–18]

Tungsten (W) is a strong ferrite former, and is effective for precipitate refining and solid solution strengthening. W is usually added to steels to improve their mechanical properties. Klueh *et al.*[19] studied the effect of W on the toughness of bainitic steels. He found that W alloying improves the hardenability of steels, and the impact property of the more hardenable 3Cr-3WV steel is better than that of 3Cr-2WV steel. The study of Suk[20] showed that an increase in W content enhanced the yield strength, which was accompanied by decreasing elongation and Charpy impact energy, and there was an optimum W content for a good combination of high yield strength with good Charpy impact energy. W induced the formation of residual ferrite and thus improved the high-temperature strength of 9CrODS steels when the W content was no more than a certain value.[21] For the Fe-8Mn-7Ni-W alloys, the tensile strength significantly increased with increasing W content at the expense of tensile elongation.[22] The study of Park *et al.*[23] indicated that the tensile strength was increased at both room and high temperatures, which was due not only to the solid solution hardening, but also to the refinement of various precipitates.

Although W addition is popular for improving the mechanical properties of steels, the studies have still been limited to the effects of W on the steel's microstructure, hardness, sag resistance, room temperature tensile strength and impact toughness, and some additional properties, such as fatigue and creep, and the studied materials are stainless steels, oxide dispersion-strengthened ferritic steels, maraging steels, *etc.*[19–26] For microalloyed forging steels with different W contents, however, the microstructural evolution, hardness, and mechanical properties have not been well reported, and their detailed mechanisms are not clearly understood. In particular, with the application of microalloyed forging steels in limited cold environments, the study of the low-temperature mechanical properties has been becoming more and more important. In the current study, several forging steels with a varying W contents were produced by a controlled forging process. The objective of the current study is to systematically investigate the effects of W addition on the microstructure, hardness, and room/low-temperature tensile properties, with a specific discussion on the mechanism of microstructural evolution and the variation in their mechanical properties.

II. EXPERIMENTAL PROCEDURE

A. *Materials*

Four kinds of steels with different W contents (0, 0.1, 0.5, and 1 wt pct) were used in the current study. The chemical compositions of the steels are shown in Table I. Ingots were homogenized at 1503 K (1230 °C) for 1 hour and then hot forged into a cuboid with section size of 140 mm × 140 mm and height of 400 mm, followed by air cooling. The final forging temperature was controlled to be higher than 1223 K (950 °C). Specimens were prepared along the height direction of the forged pieces.

B. *Tests on Mechanical Properties*

Tensile specimens were prepared according to ASTM E 8M (gauge length 30 mm, and gauge diameter 6 mm). Tensile tests were performed on an INSTRON 8862 at various temperatures (room temperature, 223 K and 173 K (−50 °C and −100 °C) with strain rate of 5×10^{-3} s^{-1}. Three specimens were used in each condition for tensile tests. Low temperatures were controlled by liquid nitrogen through a very low-temperature material test chamber. The temperature was monitored throughout each tensile test. Tensile specimen was maintained in the low-temperature chamber for 5 minutes once the desired testing temperature was achieved. The deviation of testing temperatures was controlled within ±5 °C. To avoid sliding from the clamp apparatus during tensile testing, both ends of the specimens were machined to be screw threaded, as shown in Figure 1. Specimens were attached firmly to special clamps with female screw thread on the INSTRON 8862 tensile testing machine. The resulting stress–strain curves were analyzed to determine the yield strength (YS, 0.2 pct proof stress) and ultimate tensile strength (UTS). Hardness was measured with a Vickers hardness tester using a 2-kg load and 10 second dwell time, and eight indentations for every specimen were made randomly on its surface.

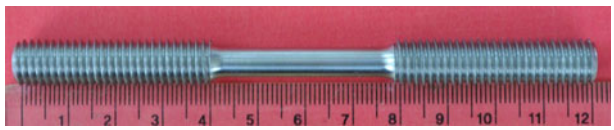

Fig. 1—Dimensions and appearance of tensile specimen used in the current study.

Table I. Chemical Compositions of the Investigated Steels (Weight Pct)

Specimens	C	Mn	Cr	Ni	Cu	Si	Al	V	Nb	Ti	P	S	N	W
0W	0.171	1.22	0.103	0.025	0.023	0.469	0.019	0.015	0.023	0.019	0.013	0.008	0.007	0
0.1W	0.170	1.20	0.103	0.024	0.024	0.471	0.024	0.015	0.023	0.020	0.014	0.009	0.008	0.09
0.5W	0.167	1.20	0.113	0.021	0.022	0.497	0.024	0.014	0.018	0.023	0.008	0.008	0.005	0.47
1W	0.171	1.20	0.112	0.024	0.022	0.499	0.021	0.016	0.020	0.020	0.008	0.008	0.006	0.99

C. *Metallography and Fractography*

Specimens were metallographically polished and etched with 2 pct nital solution for microstructural observation using an OLYMPUS BX51M optical microscope (OM). Slightly overetched specimens were examined under a JEOL JSM-6300F field-emission scanning electron microscope (FE-SEM). For observing prior austenite grain boundaries, specimens were heated to 1503 K (1230 °C) for 1 hours followed by water quenching. The water-quenched specimens were etched with a "picric acid + $FeCl_3$ + dodecyl benzene sulfonic acid sodium salt" solution to reveal prior austenite grain boundaries, and then observed by OM. To examine the character and composition of precipitates, extraction replicas, as well as thin foils mounted on Cu grids, were prepared as specimens and analyzed using the energy dispersive X-ray spectroscopy (EDS) method on a JEOL JEM-2100F transmission electron microscope (TEM) operated at 200 kV. Precipitate sizes in different W-containing steels were evaluated on five randomly selected TEM images with different numbers of precipitates. The precipitates were identified by TEM, and four particles of the same type were quantitatively analyzed by EDS to evaluate the W concentration in the precipitate. Dislocations in the specimens along the beam direction were observed by TEM, and the TEM specimens were prepared by means of a focused ion beam (FIB) technique on a FEI Quanta 3D FEG. Fracture surfaces of the tested specimens were examined by SEM using an accelerating voltage of 15 kV to determine the failure mode.

III. RESULTS AND DISCUSSION

A. *Microstructure*

1. *Microstructural observation*

Figure 2 shows the microstructure of the 0W specimen. It can be seen that the 0W specimen mainly consists of polygonal ferrite (PF) and pearlite, accompanied by a small quantity of acicular ferrite (AF). The addition of W has significantly changed the microstructures, as shown in Figure 3. Compared with the 0W specimen, the amount of AF increases after 0.1 pct W addition (Figure 3(a)). On continuously increasing W from 0.1 to 0.5 pct, a remarkable increase in the amount of AF occurs (Figure 3(b)). When the W content is increased to 1 pct, however, the microstructure consists of mixed AF and bainite ferrite (BF), as shown in Figures 3(c) and (d). The main difference between AF and BF is in their nucleation: BF is nucleated at austenite grain boundaries, while AF is intragranularly nucleated on the nonmetallic inclusions present in the steel.[27,28] The nucleated ferrite in BF forms groups of parallel plates with the same crystallographic orientation. In contrast, AF leads to a random arrangement of plates, as illustrated in Figures 3(c) and (d).

Figure 4 presents the prior austenite grains of the tested specimens. As shown in Figure 4(a), coarse-grained austenite exists in the 0W specimen. After determination by using the circular intercept method according to ASTM E112, the mean austenite grain size of 0W specimen was obtained to be 158.6 μm. The addition of W has greatly changed the austenite grain size, and increasing the W content leads to finer austenite grain size, as shown in Figures 4(b) through (d). It can therefore be concluded that W has a positive effect on retarding the growth of austenite grains. Figure 5 shows the dependence of mean prior austenite grain size on W content. As can be seen, the austenite grain size decreases slightly as the W content increases from 0 to 0.1 pct, then drops sharply when increased from 0.1 to 0.5 pct, and finally decreases gradually when the W content is higher than 0.5 pct.

2. *Characterization of precipitates*

Figure 6 shows the character and composition of precipitates in the 0W specimen. As illustrated in Figure 6(a), six precipitates are found at the current magnification. Two types of precipitates, *i.e.*, rectangular and irregular precipitates, can be classified by shape. Additional EDS analysis shows that the rectangular particles contain Ti, Nb, and V, while only Ti and Nb are found in the irregular particles, as shown in Figures 6(b) and (c). Based on the chemical compositions given in Table I and prior study,[5,29,30] the precipitates are probably Ti, Nb, and V carbides or carbonitrides. Moreover, because of the presence of the

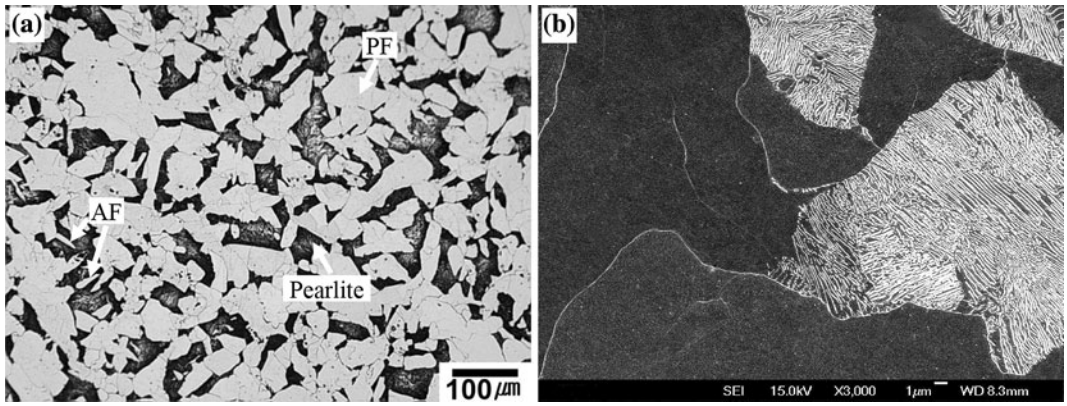

Fig. 2—Microstructure of the 0W specimen: (*a*) OM structure and (*b*) SEM of pearlite.

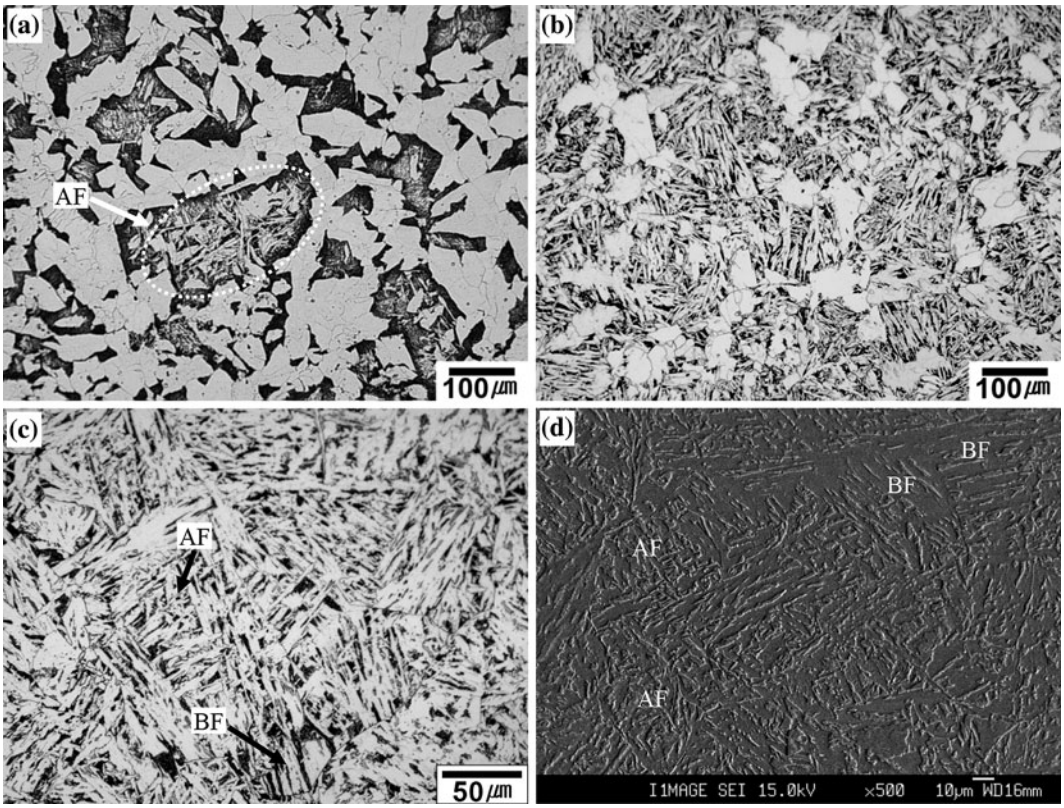

Fig. 3—OM (*a*, *b*, *c*) and SEM (*d*) structures of the W-containing specimens: (*a*) 0.1W, (*b*) 0.5W, and (*c*, *d*) 1W.

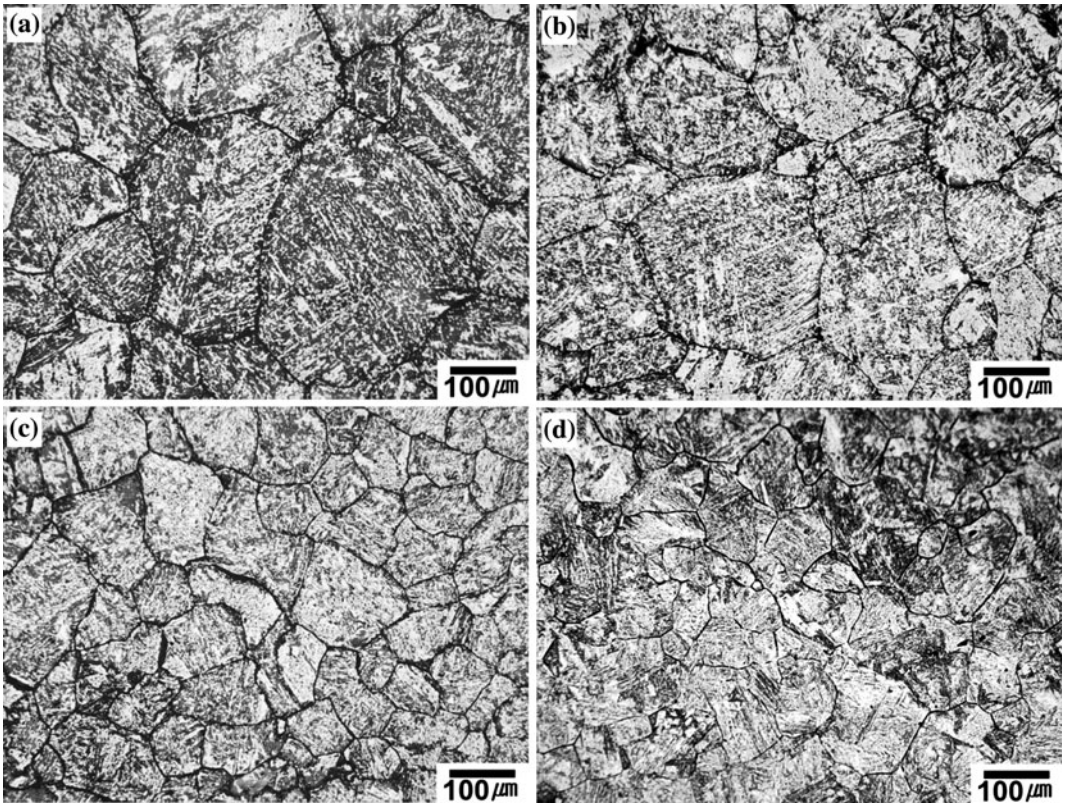

Fig. 4—Prior austenite grains of the W-containing specimens: (*a*) 0W, (*b*) 0.1W, (*c*) 0.5W, and (*d*) 1W.

Cu grid while making extraction replica specimens, both spectra show high Cu peaks.

Figure 7 shows the character and composition of precipitates in the W-containing specimens. In the case of same magnification with that of the 0W specimen, seven, five, and seven precipitates are found in the 0.1, 0.5, and 1W specimens, respectively, as shown in Figures 7(a), (d) and (g). It is clear that the addition of W does not have a noticeable effect on the amount of precipitates. EDS analysis shows that W exists in both rectangular and irregular precipitates (Figures 7(b), (c), (e), (f), (h), and (i)). In addition, an Si peak appears in all the spectra. The Si peak corresponds to silica or silicic acid formed by oxidation and hydration of the Si in the steel during the electrochemical extraction.[31] Figure 8 shows the variation of mean precipitate size with W content. It can be seen that the precipitate size decreases slowly after 0.1 pct W addition, then drops sharply when the W content is increased from 0.1 to 0.5 pct, and again decreases slowly when the W content is higher than 0.5 pct. The concentration of W in the different precipitates is presented in Table II. Based on Table II, the concentration of W in rectangular precipitates is higher than that in irregular ones in the same specimen. Also, it is obvious that the concentration of W in both rectangular and irregular precipitates increases gradually with W. According to these results, it is believed that increasing W content results in higher W concentration in precipitates, which subsequently retards the growth of such precipitates.[23] In microalloyed steels, the austenite grain growth behavior is closely related to the state of precipitates. Fine precipitates effectively inhibit austenite growth, and the finer the precipitates, the more effectively the austenite grain growth is inhibited.[32,33] Therefore, W addition induces refined precipitates which play a role in the refinement of austenite grains, as shown in Figure 4.

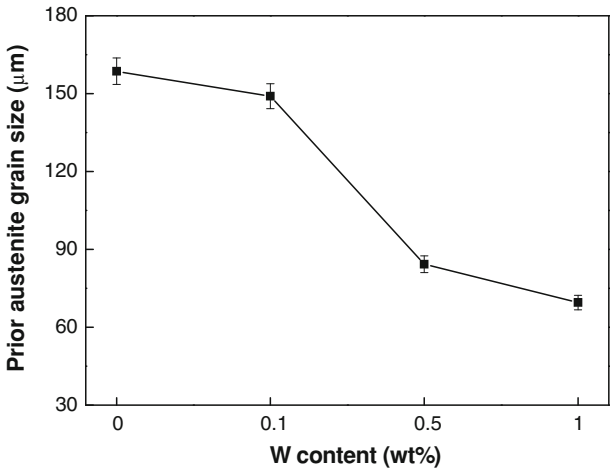

Fig. 5—Variation of prior austenite grain size with W content.

3. *Mechanism of microstructural evolution*

The term "acicular ferrite" (AF) was first used by Grong[34] and Abson[35] in 1986. AF usually forms in forged and welded steels, and the term "acicular" means shaped and pointed like a needle, but the true shape is that of a lenticular plate. AF nucleation takes place inside the austenite grains on nonmetallic inclusions. Nonmetallic inclusions can be oxides or other compounds, such as carbides/carbonitrides in microalloyed steels, but the important point is that they may stimulate AF.[36] Nonmetallic inclusions are necessary for the formation of AF. Steel which contains relatively large numbers of inclusions can provide abundant sites for AF nucleation, and then higher content of AF in the microstructure can be obtained. The nucleation of a single plate on an inclusion can in turn stimulate others to nucleate autocatalytically, so that a one-to-one correspondence between the number of active inclusions and the number of AF plates is not expected.[37] The plates of AF nucleate heterogeneously on small nonmetallic inclusions and radiate in many different directions from these point nucleation sites. AF does not grow in sheaves because their development is stifled by the impingement of plates nucleated independently at adjacent sites.[38] Since AF

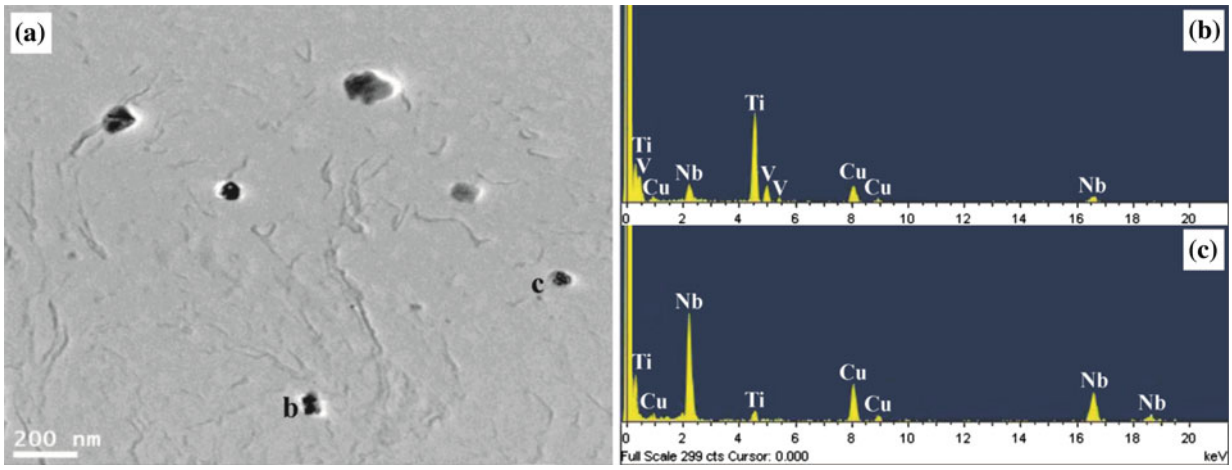

Fig. 6—Character and composition of precipitates in the 0W specimen: (*a*) TEM bright-field image, (*b*) EDS of particle "b", and (*c*) EDS of particle "c".

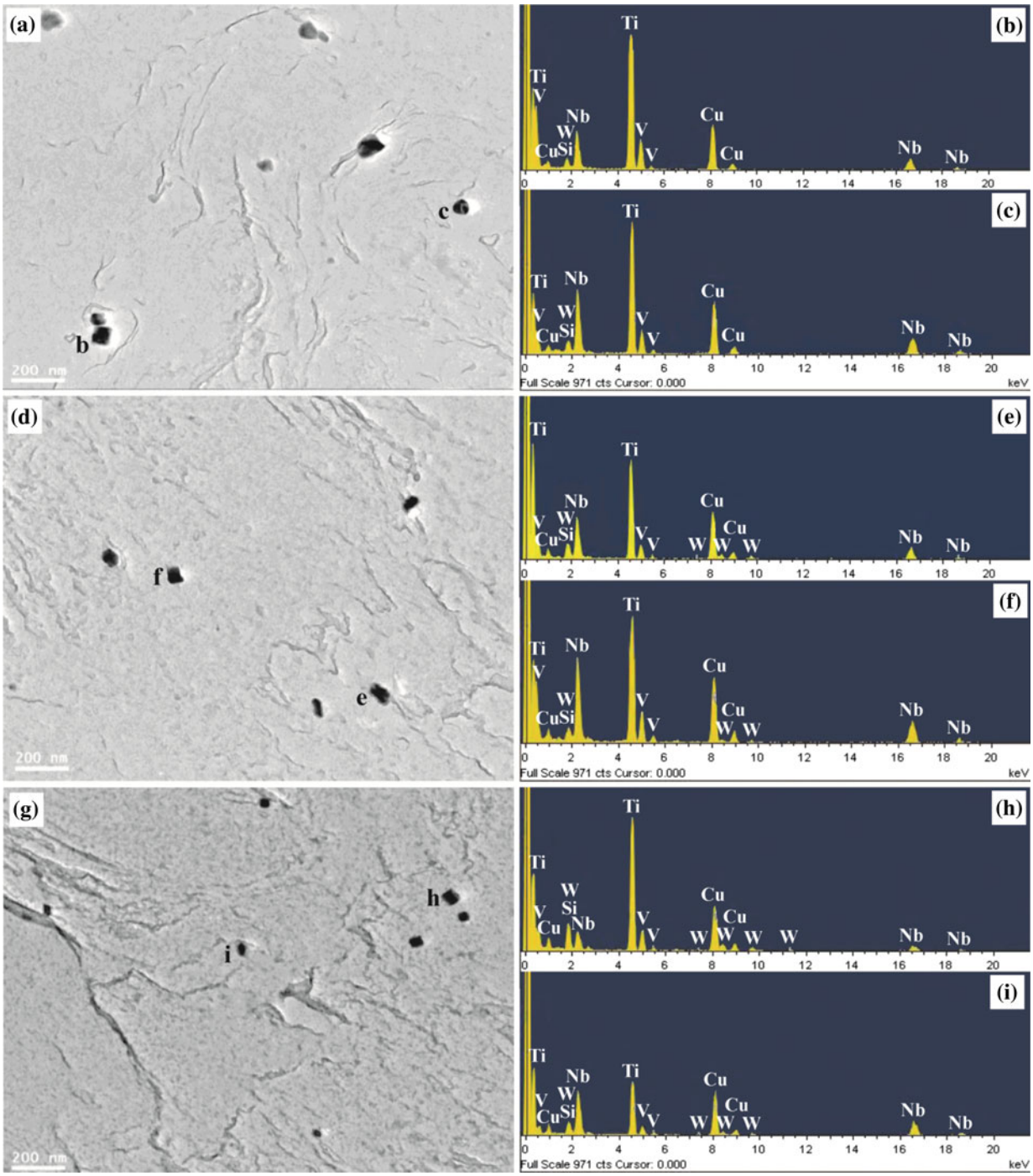

Fig. 7—Character and composition of precipitates in the (*a*, *b*, *c*) 0.1W, (*d*, *e*, *f*) 0.5W, and (*g*, *h*, *i*) 1W specimens: (*a*, *d*, *g*) TEM bright-field images, (*b*) EDS of particle "b", (*c*) EDS of particle "c", (*e*) EDS of particle "e", (*f*) EDS of particle "f", (*h*) EDS of particle "h", and (*i*) EDS of particle "i".

grows by a displacive mechanism, plates of AF are confined to austenite grains, where they grow because the coordinated movement of atoms associated with the displacive transformation mechanism cannot be sustained across grain boundaries.[39] A schematic diagram of AF formation is presented in Figure 9.

The displacive mechanism of AF nucleation relies on the existence of arrays of dislocations. These arrays are generated in the proximity of nonmetallic inclusions because of stresses caused by differential thermal expansion. Such stresses are more difficult to accommodate for larger inclusions, making large inclusions more potent nucleation sites. Ricks *et al.*[37] studied the mechanism of AF nucleation based on classical heterophase fluctuation theory, and he found that the activation energy (G^*) for a fluctuation which is large enough to stimulate a critical nucleus depends on the inverse square of the chemical driving force, $G^* \propto \Delta G^{-2}$. According to this theory, it is

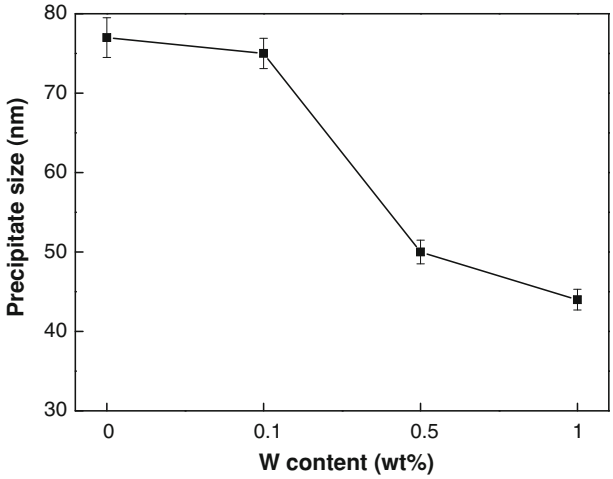

Fig. 8—Variation of precipitate size with W content.

Table II. Concentration of W in Different Precipitates (Weight Pct)

Specimens	Rectangular Precipitate	Irregular Precipitate
0W	—	—
0.1W	3.9 ± 0.22	0.9 ± 0.36
0.5W	5.3 ± 0.64	2.8 ± 0.23
1W	12.8 ± 0.45	4.7 ± 0.82

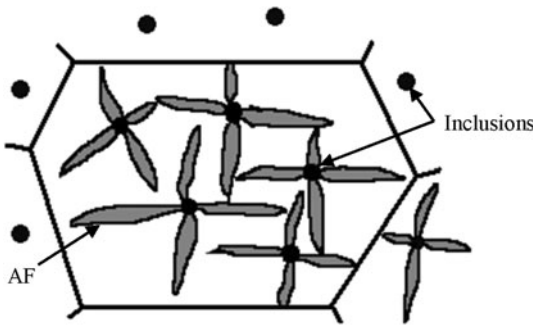

Fig. 9—Schematic diagram of AF formation.

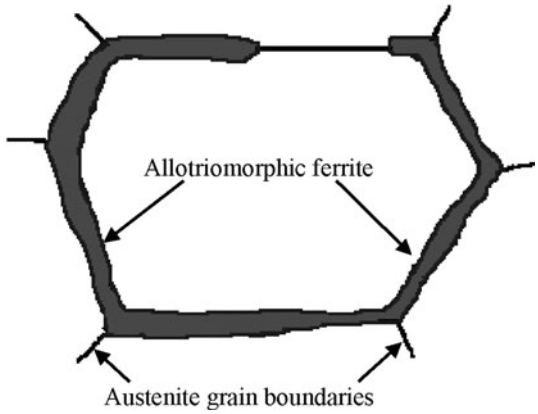

Fig. 10—Allotriomorphic ferrite formed at austenite grain boundaries.

clear that larger-sized nonmetallic inclusions are more effective for heterogeneous AF nucleation. Beside nonmetallic inclusions, another factor, the austenite grain size, is also responsible for the formation of AF. AF is intragranularly nucleated BF, and it is possible to switch between these two morphologies by controlling the nucleation sites. The appearance of AF is only different from that of BF because it nucleates intragranularly in steels containing a greater number density of inclusions than austenite grain surface nucleation sites.[38] BF forms when the austenite grain size is small because nucleation then predominates at the grain boundaries. Subsequent growth then swamps the interiors of austenite grains, preventing the development of AF. A microstructure with large austenite grains has a better chance of transformation to AF at the expense of BF because the number density of inclusions becomes large enough relative to the boundary nucleation sites.

According to the analysis results on precipitates and prior austenite grains, there are no noticeable increases in the amounts of precipitates after W addition compared with the specimen without W (Figures 6 and 7), and the mean sizes of both austenite grains and precipitates decrease with increasing W content (Figures 5 and 8). Obviously, these factors are not beneficial to the formation of AF. Another factor, allotriomorphic ferrite, is then considered to analyze the effects of W on the development of AF in mixed microstructures. Allotriomorphic ferrite is the first phase to form on cooling the austenite grains less than the Ae_3 temperature.[40] Nucleation takes place at the columnar austenite grain boundaries. Because these boundaries are easy diffusion paths, they become decorated with thin, continuous layers of ferrite (Figure 10). From our observation, allotriomorphic ferrite can scarcely be found in the 0W specimen (Figure 2). Conversely, the amount of allotriomorphic ferrite increases gradually with W content from 0 to 0.5 pct, and the addition of 0.5 pct W induces the highest volume fraction of allotriomorphic ferrite to be formed in the microstructure (Figures 3(a) and (b)). Figure 11 shows an SEM image of allotriomorphic ferrite formed in the 0.5W specimen at higher magnification. It can be seen that the shape of the allotriomorphic ferrite is very intact, which means the austenite grain surfaces are probably entirely covered by allotriomorphic ferrite. When the W content is increased to 1 pct, however, no allotriomorphic ferrite can be found in the microstructure, as shown in Figures 3(c) and (d). Therefore, when the W content is no greater than a certain value, it can favor the formation of allotriomorphic ferrite.

AF is intragranularly nucleated BF, and the formation of allotriomorphic ferrite is favorable to the development of AF instead of BF because the austenite grain surface sites for BF nucleation are covered by allotriomorphic ferrite, and the austenite grain boundaries are then not free to nucleate BF.[41,42] In the current study, the amount of allotriomorphic ferrite increases gradually with W when its content is lower

than 0.5 pct, and the volume fraction of AF consequently increases. When the content of W is high (>0.5 pct), the formation of BF in the microstructure may be related to the reduction in the coverage of austenite grain boundaries by layers of allotriomorphic ferrite, so that the austenite grain boundaries are then freed for BF nucleation. When less than 0.5 pct W, the steel hardenability is low enough to insure that the austenite grain surfaces are completely covered by uniform layers of allotriomorphic ferrite, thereby rendering them useless for BF nucleation, and consequently allowing the development of AF by intragranular transformation. As the W content increases, some of the austenite grain surfaces are left bare and become available for the formation of BF sheaves, as soon as the temperature falls within the bainite transformation range. Also, at relatively higher W content, the sizes of austenite grains and precipitates are small, favoring the formation of BF instead of AF. The mechanism of the transition from AF to BF is schematically illustrated in Figure 12.

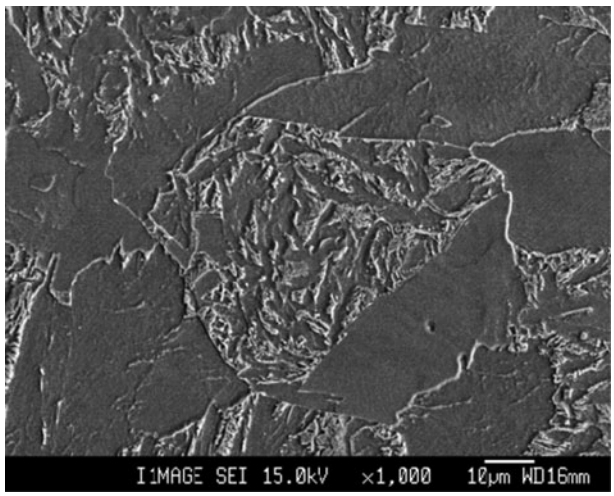

Fig. 11—SEM image of allotriomorphic ferrite formed in the 0.5W specimen.

B. *Mechanical Properties*

1. *Tensile behavior and hardness*

Figures 13(a) through (c) present the typical tensile curves of the tested specimens at room temperature (RT), 223 K and 173 K (−50 °C and −100 °C), respectively. The tensile properties determined from these curves along with the hardness are listed in Table III. The relationships between tensile properties and W contents at various temperatures are presented in Figure 14.

The results show that the tensile behaviors at RT are similar to those at 223 K (−50 °C), *i.e.*, all the engineering stress *vs* strain curves without apparent yield points can be simply divided into three stages, such as elastic deformation, plastic deformation, and fracture, as shown in Figures 13(a) and (b). With the temperature continuously decreasing from 223 K to 173 K (from −50 °C to −100 °C), the tensile behavior is greatly changed. As shown in Figure 13(c), the tensile curves at 173 K (−100 °C) exhibit lower strain to failure compared with those at RT and 223 K (−50 °C).

From Table III and Figure 14, it can be found that the addition of W brings about increases in both the hardness and the tensile strength at the expense of strain. Also, the YS and UTS of all specimens increase gradually with decreasing temperature from RT to 173 K (−100 °C) (Figure 14(a)). As demonstrated in Figure 14(b), the strain to failure is higher when tested at 223 K (−50 °C) than that at RT in the W content ranging from 0 to 0.5 pct. When the W content is increased to 1 pct, however, the fracture strain at 223 K (−50 °C) is slightly lower than that at RT. When tested at 173 K (−100 °C), the fracture strain shows a very low value relative to that at RT and −50 °C, and the fracture strain decreases moderately in the W content range of 0 to 0.5 pct, then drops sharply when the W content is higher than 0.5 pct (Figure 14(b)).

Figure 15 shows plots of the logarithms of YS and UTS as functions of the inverse of the absolute testing temperature. It is apparent that a linear relationship between $\ln\sigma$ and $1/T$ can be obtained as

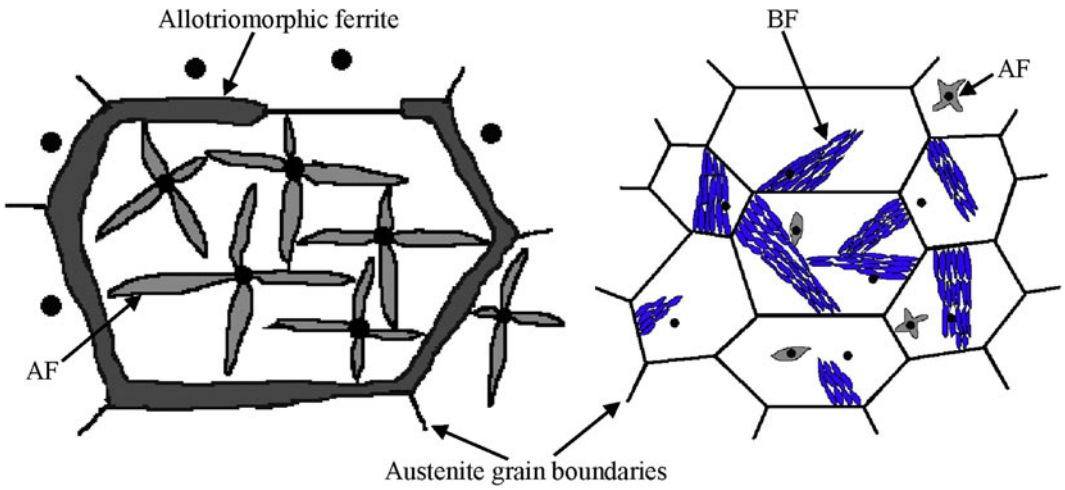

Fig. 12—Schematic illustration of the mechanism of the transition from AF to BF.

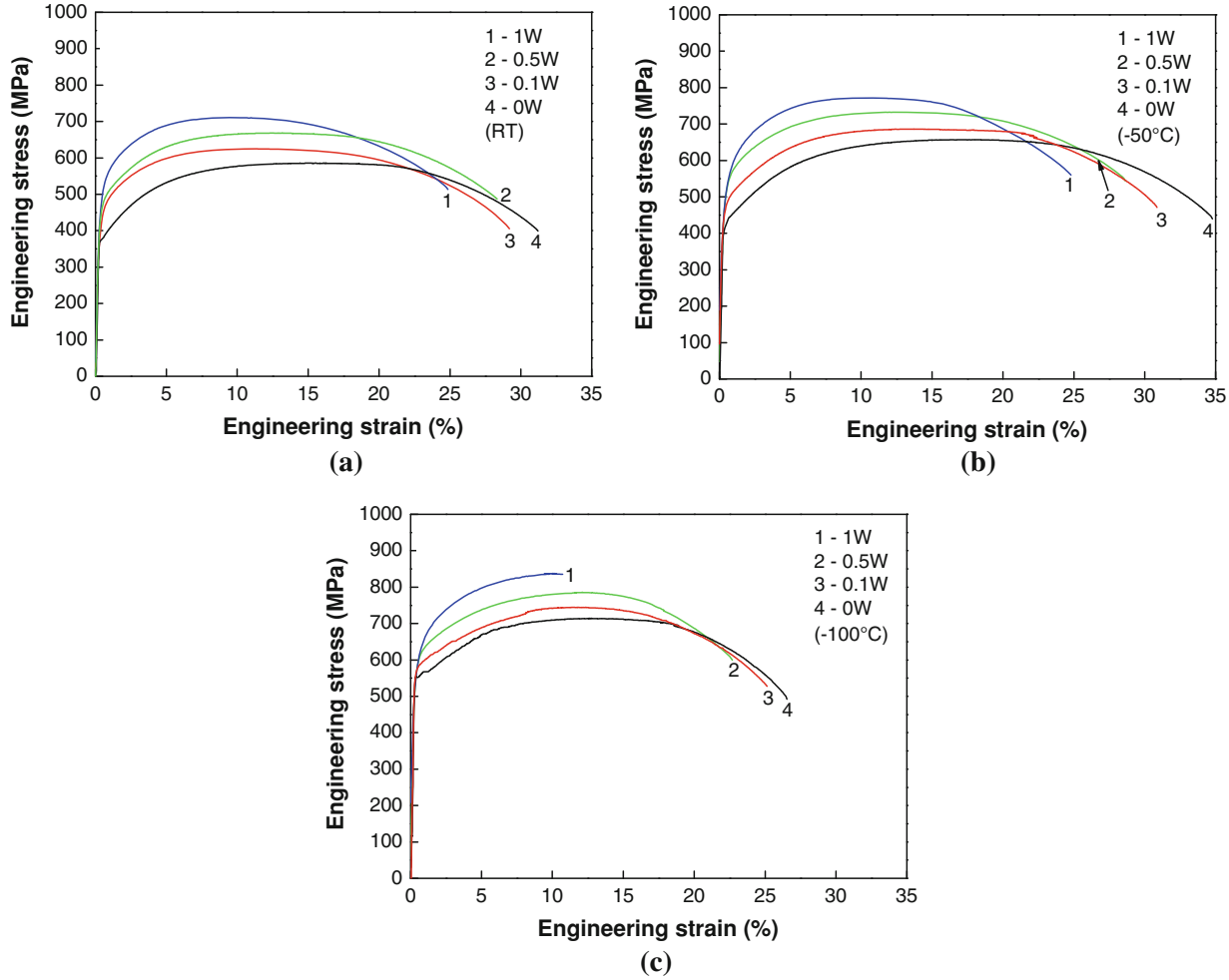

Fig. 13—Typical tensile curves of the tested specimens at (*a*) RT, (*b*) −50 °C, and (*c*) −100 °C.

Table III. Tensile Properties of the Tested Specimens at Various Temperatures

Specimens	Temperature (°C)	YS (MPa)	UTS (MPa)	Strain (pct)	Hardness (HV2)
0W	RT	299.1	585.6	31.2	185
	−50	336.6	657.2	34.8	
	−100	383.7	714.1	26.5	
0.1W	RT	313.4	624.9	29.2	217
	−50	365.4	686.2	30.9	
	−100	409.8	744.4	25.1	
0.5W	RT	345.7	668.2	28.3	223
	−50	379.8	732.6	28.6	
	−100	424.6	785.6	22.7	
1W	RT	351.9	711.1	24.9	232
	−50	392.2	771.7	24.8	
	−100	439.1	837.6	10.7	

$$\ln\sigma = \ln A + n/T \quad [1]$$

where σ is the stress, T is the absolute testing temperature, and A and n are constants. Then, the stress can be expressed as an Arrhenius type function of T as: $\sigma = Ae^{n/T}$. After linear regression from Figure 15, the values of $\ln A$ and n of the tested specimens with different contents of W can be obtained, as illustrated in Table IV. Such relationships between σ and T can be used to estimate the YS and UTS of the steels at other testing temperatures.

2. *Fractography*

Figure 16 shows the fracture surfaces of specimens tested at RT and 223 K (−50 °C). When tested at RT, the fracture surfaces of all the specimens with different W contents are

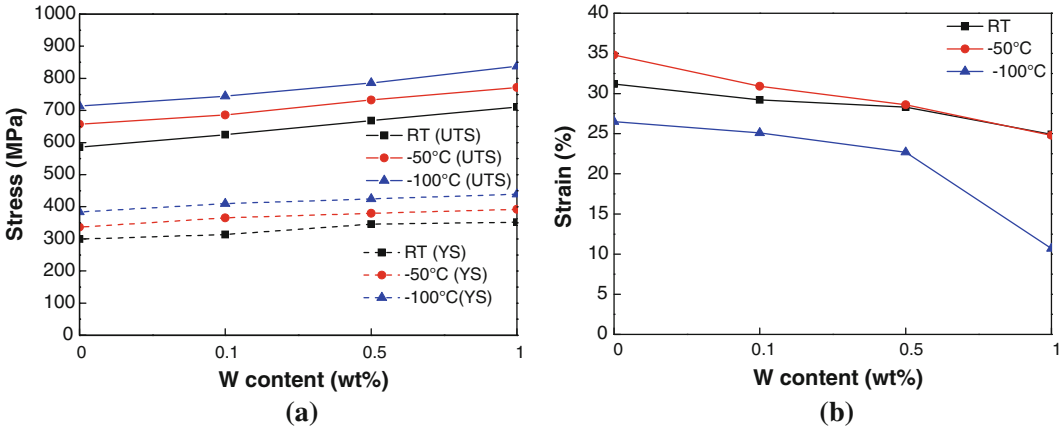

Fig. 14—Relationships between tensile properties and W contents at various temperatures: (*a*) plots of stress *vs* W content, and (*b*) plots of strain *vs* W content.

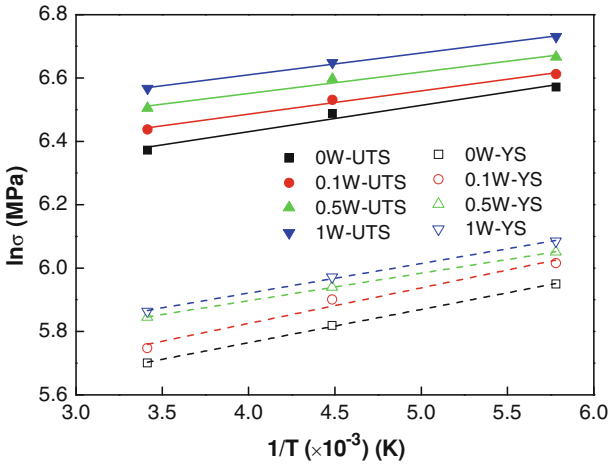

Fig. 15—Plots of lnσ *vs* 1/T of specimens with different W contents.

Table IV. Values of ln*A* and *n* of the Tested Specimens

Stress	Constants	0W	0.1W	0.5W	1W
YS	ln*A*	5.344	5.375	5.550	5.548
	n	0.105	0.112	0.087	0.093
UTS	ln*A*	6.098	6.192	6.280	6.334
	n	0.083	0.074	0.068	0.069

composed of dimples, which indicate a characteristic of ductile fracture. Also, the size of dimples decreases with the increase of W content (Figures 16(a) through (c)). As temperature decreases from RT to 223 K (−50 °C), the fracture modes of some specimens have been changed. As shown in Figures 16(d) and (e), the fracture surfaces of both the 0 and 0.5W specimens still show the ductile mode. However, when the W content is increased to 1 pct, the fracture surface is mixed with cleavage facets and small dimples (Figure 16(f)). Moreover, with decreasing temperature from RT to 223 K (−50 °C), the size of the dimples shows a decreasing trend.

Figure 17 shows the fracture surfaces of specimens tested at 173 K (−100 °C). As illustrated in Figures 17(a) through (c) at low magnification, the necking phenomenon becomes less and less obvious with increasing W content, indicating a decreasing trend of strain with W after tensile testing. The fracture feature of the 0 W specimen still shows a ductile mode (Figure 17(d)). As shown in Figure 17(e), however, the fracture surface of the 0.5W specimen consists of cleavage facets, small dimples, and small quantities of cracks. When the W content is increased to 1 pct, the fracture surface becomes a mixture of cleavage facets and many short cracks, which means that full brittle fracture has occurred (Figure 17(f)). Comparing Figure 17(f) with Figure 16(f), it follows that the ductile-to-brittle transition (DBT) of the 1W specimen took place when the temperature decreased from 223 K to 173 K (from −50 °C to −100 °C).

Table V presents the characteristics of fracture surfaces of the specimens tested at various temperatures. As can be seen, specimens with higher W content exhibit higher temperature to DBT. Moreover, based on Table V, it can be deduced that the 0.5W specimen will be the next one to experience DBT as the temperature continuously decreases from 173 K (−100 °C) to a much lower one. According to the above fracture surface examination and analysis, it can be concluded that the addition of W has a positive effect on increasing the DBT temperature.

3. *Discussion on the variation of mechanical properties*

When the W content is increased from 0 to 0.5 pct, the amount of allotriomorphic ferrite increases gradually, which subsequently leads to an increase in the volume fraction of AF. The shape change is always associated with the growth of AF, and such shape deformation causes plastic deformation in the adjacent austenite. As reported by Strangwood,[43] the resulting dislocations are inherited by the AF as it grows, giving a dislocation density which is typically at $10^{14}\,m^{-2}$, and which contribute some 145 MPa to its strength. Figures 18(a) and (b) contain TEM micrographs of dislocations in ferrite observed in the 0 and 0.1W specimens, respectively. It can be seen that large numbers of dislocations exist in the 0.1W specimen relative to that in the 0W specimen, and hence, higher hardness and strength of the 0.1W specimen are expected. When the W content is increased to 1 pct, allotriomorphic ferrite

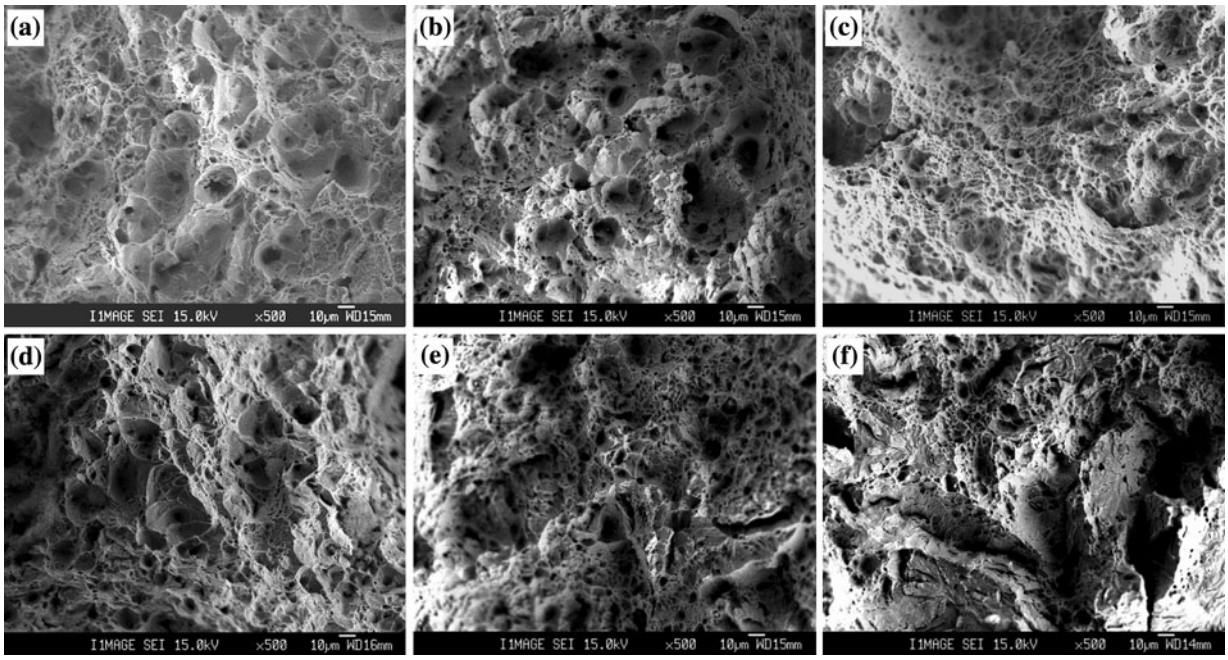

Fig. 16—Fracture surfaces of specimens tested at (*a*, *b*, *c*) RT and (*d*, *e*, *f*) −50 °C: (*a*, *d*) 0W, (*b*, *e*) 0.5W, and (*c*, *f*) 1W.

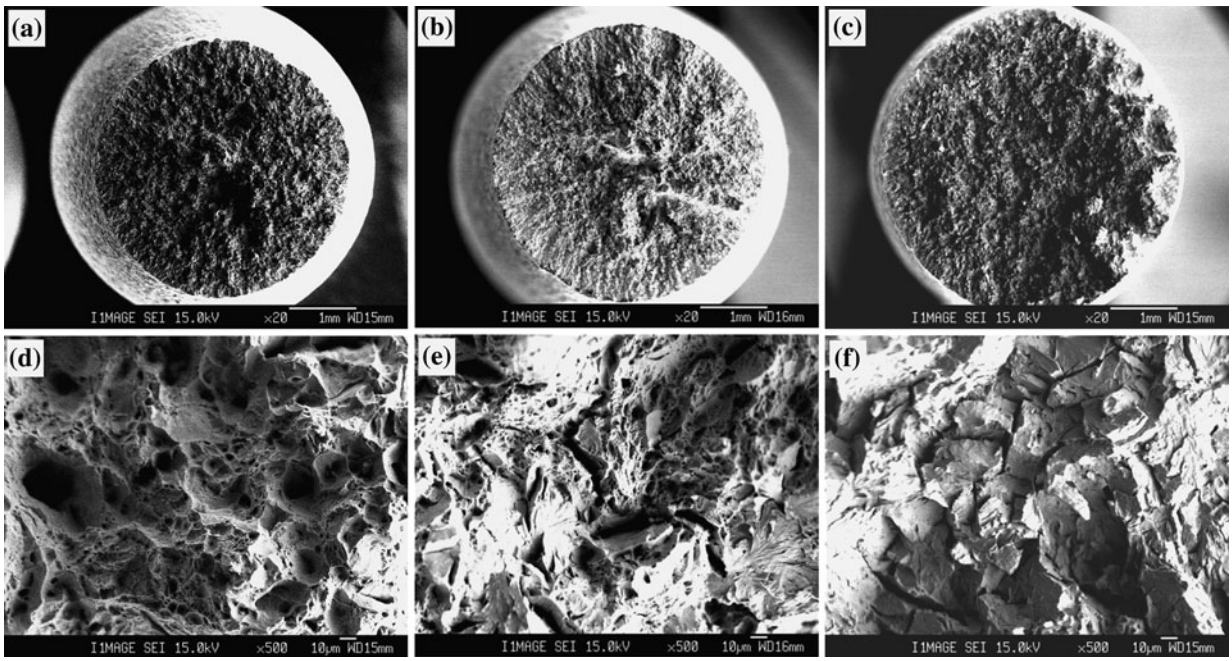

Fig. 17—Fracture surfaces of specimens tested at −100 °C: (*a*, *d*) 0W, (*b*, *e*) 0.5W, and (*c*, *f*) 1W.

Table V. Characteristics of Fracture Surfaces of the Specimens Tested at Various Temperatures

Temperatures (°C)	0W	0.1W	0.5W	1W
RT	D	D	D	D
−50	D	D	D	D + CF
−100	D	D	D + CF + C	CF + C

D: dimples; *CF*: cleavage facets; and *C*: cracks.

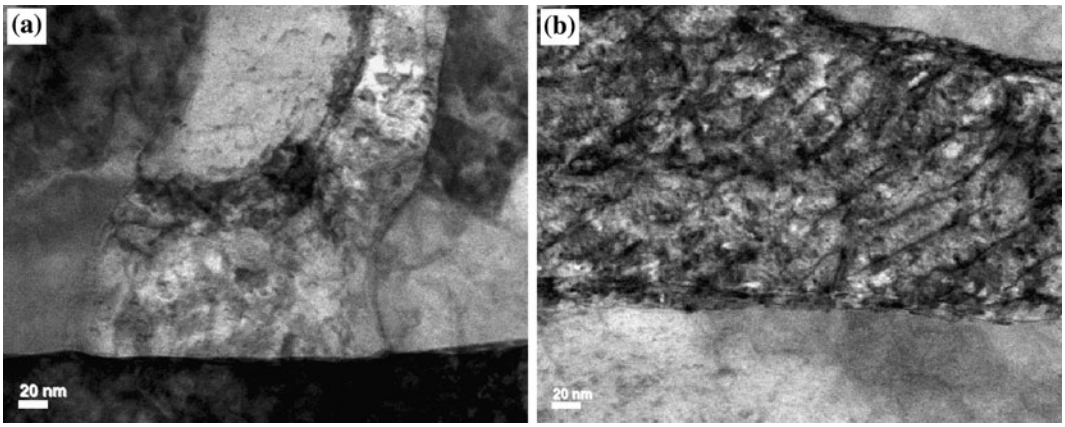

Fig. 18—TEM micrographs of dislocations in ferrite observed in (*a*) 0W and (*b*) 0.1W specimens.

disappears, and the microstructure consists of mixed AF and BF. The TEM results obtained by Smith[44] revealed that the dislocation density of bainite ρ_d is about 4×10^{14} m^{-2}, which is higher than that of allotriomorphic ferrite obtained in the same steel with $\rho_d \approx 0.5 \times 10^{14}$ m^{-2}. In another supporting experiment, similar results for the dislocation densities of bainite and allotriomorphic ferrite were measured to be 1.7×10^{14} and 0.37×10^{14} m^{-2}, respectively.[45] It then follows that bainite contains more dislocations than allotriomorphic ferrite, thus improving the hardness and strength. As regards the reasons for the increase in hardness and strength after W addition, the following other causes are considered. One is the solid solution strengthening induced by W addition, which results from the fact that the atomic size of W is about 10 pct larger than that of Fe. The other is the hardening induced by the fine precipitates in W-containing steels. With refinement of various precipitates, the barriers to dislocation motion increase with the increasing amount of interphase boundaries, leading to an increase in the hardness and strength in this way.

At low temperatures, the flow stress of steels has been found to be strongly temperature dependent, as in other body-centered cubic (BCC) and BCC-like materials.[46–48] As the temperature decreases, the increases in both YS and UTS are largely attributed to the larger effective stress needed to move the dislocations past short-range obstacles at low temperatures as sufficient thermal energy for dislocation motion is lacking.[49] For BCC materials, it is well accepted that the low-temperature plastic deformation behavior is controlled by a Peierls lattice resistance mechanism.[50–53] In the Peierls mechanism, the dislocations experience the periodicity of the lattice as glide on their slip plane, which results in the presence of peaks and valleys of energy as a function of dislocation position. A moving dislocation causes bond angle distortions. BCC materials are strongly directional in their bonding, and the bond angle distortion necessary for dislocation motion in these materials is thus difficult to overcome. In BCC materials, the Peierls force is the primary obstacle to dislocation motion, even when lattice vibration energy is enhanced at high temperatures. BCC materials develop a directional bonding component at low temperatures. The movement of dislocations in BCC materials is thus strongly inhibited at low temperatures by the Peierls force. It is therefore expected that the strength of the studied steels, which are BCC structures, would exhibit an increasing trend with decreasing testing temperature. Because the matrix is highly dislocated, it would have large numbers of mobile dislocations even at low temperatures. The presence of these mobile dislocations would tend to limit the tendency toward cleavage and permit slip to take place;[47] there would therefore be resistance to necking in tensile tests, and good strain values would be exhibited, particularly at 223 K (−50 °C). Since the dislocation motion is retarded with the refinement of precipitates after W addition, the increment of strain at 223 K (−50 °C) relative to that at RT shows a decreasing trend with W (Figure 14(b)). When the testing temperature is decreased to 173 K (−100 °C), the sharp decrease in strain is probably caused by the considerable reduction in mobile dislocations at such low temperature.

IV. CONCLUSIONS

Microalloyed forging steels with different microstructures were produced by varying the additions of W, and their microstructure, hardness, and room/low-temperature tensile properties were systematically analyzed.

1. The effect of W addition on the amount of precipitates was not noticeable. The precipitates in W-containing steels were all rich in W, and the W concentration in the precipitates increased with the increasing W content. The sizes of both austenite grains and precipitates decreased with the increasing W content.
2. When the W content was equal to or less than 0.5 pct, the addition of W favored the formation of allotriomorphic ferrite, which subsequently promoted the development of AF in microalloyed forging steels.
3. W played an important role in increasing the hardness and tensile strength at the expense of strain. With decreasing testing temperature, both YS and UTS showed an increasing trend. The tensile strength was strongly temperature dependent, and the relationship between tensile strength and temperature followed an Arrhenius type equation as $\sigma = Ae^{n/T}$.

4. When the W content was equal to or less than 0.5 pct, the fracture strain at 223 K (−50 °C) was higher than that at RT. At 173 K (−100 °C), the fracture strains of all the tested specimens showed were very low relative to those at RT and 223 K (-50 °C). When the temperature decreased from 223 K to 173 K (−50 °C to −100 °C), the DBT of the specimen with 1 pct W occurred. The addition of W showed a positive effect while increasing the DBT temperature.
5. Based on the above results, it is suggested that the mechanical properties of microalloyed forging steels are closely related to the W content, and the addition of 0.5 pct W yields the best combination of excellent room/low-temperature tensile strength and ductility.

ACKNOWLEDGMENTS

This study was financially supported by the Ministry of Knowledge and Economy, Korea under the program (2009-D-2-A-Y0-B-07) of the Leading Industry Development for Dongnam Economic Region. The authors would like to thank Dr. Tania Silver from the University of Wollongong for assisting in the English editing.

REFERENCES

1. R.M.K. Honeycombe and H.K.D.H. Bhadeshia: *Steels, Microstructure and Properties,* 2nd ed., Arnold, London, 1995, p. 189.
2. D. Whittaker: *Metall.*, 1979, vol. 46, pp. 275–81.
3. M. Jahazi and B. Eghbali: *J. Mater. Process. Technol.*, 2001, vol. 113, pp. 594–98.
4. G. Krauss: *Steels: Processing Structure and Performance*, ASM International, Ohio, 2005, pp. 230–32.
5. J. Zhao, J.H. Lee, Y.W. Kim, Z. Jiang, and C.S. Lee: *Mater. Sci. Eng. A*, 2013, vol. 559, pp. 427–35.
6. S. Roy, S. Patra, S. Neogy, A. Laik, S.K. Choudhary, and D. Chakrabarti: *Metall. Mater. Trans. A*, 2012, vol. 43A, pp. 1845–60.
7. J.G. Jung, J.S. Park, J. Kim, and Y.K. Lee: *Mater. Sci. Eng. A*, 2011, vol. 528, pp. 5529–35.
8. S. Vervynckt, P. Thibaux, and K. Verbeken: *Met. Mater. Int.*, 2012, vol. 18, pp. 37–46.
9. S. Shanmugam, N.K. Ramisetti, R.D.K. Misra, T. Mannering, D. Panda, and S. Jansto: *Mater. Sci. Eng. A*, 2007, vols. 460–461, pp. 335–43.
10. Y.M. Kim, S.Y. Shin, H. Lee, B. Hwang, S. Lee, and N.J. Kim: *Metall. Mater. Trans. A*, 2007, vol. 38A, pp. 1731–42.
11. G. Huang and K.M. Wu: *Met. Mater. Int.*, 2011, vol. 17, pp. 847–52.
12. C.P. Reip, S. Shanmugam, and R.D.K. Misra: *Mater. Sci. Eng. A*, 2006, vol. 424, pp. 307–17.
13. B.K. Show, R. Veerababu, R. Balamuralikrishnan, and G. Malakondaiah: *Mater. Sci. Eng. A*, 2010, vol. 527, pp. 1595–1604.
14. S. Sankaran, Gouthama, S. Sangal, and K.A. Padmanabhan: *Metall. Mater. Trans. A*, 2006, vol. 37A, pp. 3259–73.
15. D. Rasouli, Sh. Khameneh Asl, A. Akbarzadeh, and G.H. Daneshi: *J. Mater. Process. Technol.*, 2008, vol. 206, pp. 92–98.
16. C. Capdevila, F.G. Caballero, and C. García de Andrés: *Metall. Mater. Trans. A*, 2001, vol. 32A, pp. 661–69.
17. C. Caminaga, W.J. Botta Filho, M.L.N. Silva, and S.T. Button: *Procedia Eng.*, 2011, vol. 10, pp. 512–17.
18. M.A. Suarez, M.A. Alvarez-Pérez, O. Alvarez-Fregoso, and J.A. Juarez-Islas: *Mater. Sci. Eng. A*, 2011, vol. 528, pp. 4924–26.
19. R.L. Klueh, D.J. Alexander, and P.J. Maziasz: *Metall. Mater. Trans. A*, 1997, vol. 28A, pp. 335–45.
20. J.I. Suk, C.N. Park, S.H. Hong, and Y.G. Kim: *Mater. Sci. Eng. A*, 1991, vol. 138, pp. 367–73.
21. T. Narita, S. Ukai, S. Ohtsuka, and M. Inoue: *J. Nucl. Mater.*, 2011, vol. 417, pp. 158–61.
22. N.H. Heo and H.C. Lee: *Scripta Metall. Mater.*, 1995, vol. 33, pp. 2031–35.
23. J.S. Park, S.J. Kim, and C.S. Lee: *Mater. Sci. Eng. A*, 2001, vol. 298, pp. 127–36.
24. S.G. Hong, W.B. Lee, and C.G. Park: *J. Nucl. Mater.*, 2001, vol. 288, pp. 202–07.
25. S.B. Kim, K.W. Paik, and Y.G. Kim: *Mater. Sci. Eng. A*, 1998, vol. 247, pp. 67–74.
26. W.J. Nam, C.S. Lee, and D.Y. Ban: *Scripta Mater.*, 1997, vol. 36, pp. 1315–20.
27. J.R. Yang and H.K.D.H. Bhadeshia: *Mater. Sci. Technol.*, 1989, vol. 5, pp. 93–97.
28. I. Madariaga, I. Gutierrez, and H.K.D.H. Bhadeshia: *Metall. Mater.Trans. A*, 2001, vol. 32A, pp. 2187–97.
29. K. Inoue, N. Ishikawa, and K. Ishida: *ISIJ Int.*, 2001, vol. 41, pp. 175–82.
30. R.M. Poths, R.L. Higginson, and E.J. Palmiere: *Scripta Mater.*, 2011, vol. 44, pp. 147–51.
31. R.W. Gurry, J. Christakos, and C.D. Stricker: *Trans. ASM*, 1958, vol. 50, pp. 105–28.
32. J. Zhao, Z. Jiang, J.S. Kim, and C.S. Lee: *Mater. Des.*, 2013, vol. 49, pp. 252–58.
33. J. Zhao, Z. Jiang, and C.S. Lee: *Mater. Des.*, 2013, vol. 47, pp. 227–33.
34. O. Grong and D.K. Matlock: *Int. Met. Rev.*, 1986, vol. 31, pp. 27–48.
35. D.J. Abson and R.J. Pargeter: *Int. Met. Rev.*, 1986, vol. 31, pp. 141–94.
36. Y. Ito and M. Nakanishi: *Sumitomo Search*, 1976, vol. 15, pp. 42–62.
37. R.A. Ricks, P.R. Howell, and G.S. Barritte: *J. Mater. Sci.*, 1982, vol. 17, pp. 732–40.
38. J.R. Yang and H.K.D.H. Bhadeshia: in *Advances in Welding Science and Technology*, S.A. David, ed., ASM, Metals Park, OH, 1987, pp. 187–91.
39. H.K.D.H. Bhadeshia: *Bainite in Steels*, 2nd ed., The University Press, Cambridge, London, 2001, p. 239.
40. H.K.D.H. Bhadeshia and R.W.K. Honeycombe: *Steels: Microstructure and Properties*, 3rd ed., Elsevier Butterworth-Heinemann, Oxford, 2006, p. 291.
41. G. Snieder and H.W. Kerr: *Can. Metall. Quart.*, 1984, vol. 23, pp. 315–25.
42. S.S. Babu and H.K.D.H. Bhadeshia: *Mater. Sci. Technol.*, 1990, vol. 6, pp. 1005–20.
43. M. Strangwood and H.K.D.H. Bhadeshia: in *Advances in Welding Science and Technology*, S.A. David, ed., ASM, Metals Park, OH, 1987, pp. 209–13.
44. G.M. Smith: Ph.D. Thesis, University of Cambridge, 1984.
45. M.K. Graf, H.G. Hillenbrand, and P.A. Peters: *Accelerated Cooling of Steel*, P.D. Southwick, ed., TMS-AIME, Warrendale, 1985, pp. 349–66.
46. W.A. Spitzig and A.S. Keh: *Acta Metall.*, 1970, vol. 18, pp. 1021–33.
47. M.R. Krishnadev and R. Ghosh: *Metall. Trans. A*, 1979, vol. 10A, pp. 1941–44.
48. S. Naamane, G. Monnet, and B. Devincre: *Int. J. Plast*, 2010, vol. 26, pp. 84–92.
49. W.A. Spitzig and A.S. Keh: *Metall. Trans.*, 1970, vol. 1, pp. 3325–31.
50. C. Keller, M.M. Margulies, Z. Hadjem-Hamouche, and I. Guillot: *Mater. Sci. Eng. A*, 2010, vol. 527, pp. 6758–64.
51. S. Vaynman, M.E. Fine, S. Lee, and H.D. Espinosa: *Scripta Mater.*, 2006, vol. 55, pp. 351–54.
52. P. Spätig, G.R. Odette, and G.E. Lucas: *J. Nucl. Mater.*, 1999, vol. 275, pp. 324–31.
53. B.A. Hands and H.M. Rosenberg: *Acta Metall.*, 1969, vol. 17, pp. 455–61.